

Supporting Information

**Solvated-Electron Production by Cyanocuprates is Compatible with the UV-environment on a Hadean-Archaeon Earth**

*Zoe R. Todd, Albert C. Fahrenbach, Christopher J. Magnani, Sukrit Ranjan, Anders Björkbom, Jack W. Szostak, and Dimitar D. Sasselov*

Table of Contents:

I.	General Methods	2
II.	Cyanocuprate Mechanism	5
III.	UV/Vis Spectroscopy	6
	a. Irradiation experiments analysis	6
	b. Dicyanocuprate vs. tricyanocuprate	8
	c. Copper control experiments	11
IV.	Cyanide Electrode Monitoring	13
V.	LC-MS	17
VI.	Atmospheric Modeling	21
VII.	Tables of Experimental Values	22
VIII.	References	23

## I. General Methods

Potassium cyanide (KCN; 98%) and copper cyanide (CuCN; 99%) were purchased from Sigma-Aldrich. The solutions for the irradiation experiments all contained 0.0625 mM CuCN and 0.125 mM KCN. All solutions were prepared anaerobically in a glove box (Coy Labs PureLab 2GB Glovebox System) filled with an inert gas mixture (98% N<sub>2</sub>, 2% H<sub>2</sub>). To bring materials and solutions in and out of the glove box, an airlock system was used, with two cycles of purging to ensure oxygen removal. One cycle of purging constitutes 3 times of purging with nitrogen and one time with the nitrogen-hydrogen gas mixture. To make the solutions, a stock solution of 1 M KCN, 0.5 M CuCN was prepared. The pH of the solution was adjusted to 7.4 by using concentrated HCl. This stock solution was then diluted 100x to a concentration of 5 mM CuCN and 10 mM KCN. This solution was then diluted again to prepare 50 mL of a solution containing 0.0625 mM CuCN and 0.125 mM KCN. The pH was checked and adjusted to 7.4, using 1 M HCl. Aliquots (1 mL) were transferred to Eppendorf tubes and frozen at -30° C in the dark until time of use.

In order to carry out an irradiation experiment, one of the samples contained in the Eppendorf tubes was first sonicated and then 0.7 mL of this solution was transferred anaerobically to a Spectrosil quartz cuvette with a screw top (Starna Cells part number 9-Q-10-GL14-C). A micro-stirbar was placed inside the cuvette. An initial UV-Vis absorption spectrum (200–350 nm) was taken before irradiation, using an Amersham Sciences Ultrospec 3100 pro. The cuvette was then placed in the tunable lamp setup, set at the appropriate wavelength and bandwidth (215–295 nm in 10 nm intervals, with 10 nm bandwidths), with stirring on. Every fifteen minutes for the first two hours, the

cuvette was removed briefly from the lamp and a UV-Vis absorption spectrum was recorded. Subsequent timepoints were taken every half hour until 3.5 hours of total irradiation had elapsed.

The tunable lamp setup consists of a 75 W Tunable PowerArc, made by Optical Building Blocks (OBB). Figure S1 shows the lamp setup. This apparatus uses a xenon arc lamp and a monochromator to allow for tunable wavelength selection. The monochromator is a diffraction grating that separates the spectrum of the lamp by wavelength. Changing the relative position of the grating and the exit slit allows for precise wavelength selection. The cuvette is held in the enclosed housing capable of magnetic stirring. The bandwidth of irradiation can also be adjusted as desired.

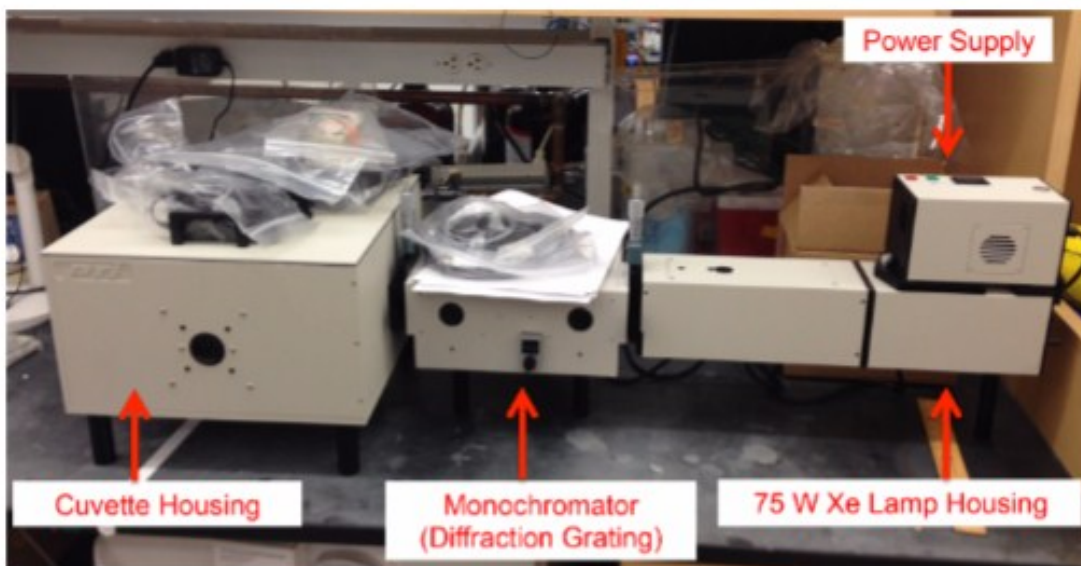


Figure S1. Optical Building Blocks 75W Tunable PowerArc lamp used for irradiation experiments with varying wavelengths. A xenon arc lamp is used in conjunction with a diffraction grating to split the light into its spectrum. Adjusting the position of the grating with respect to the exit slit allows for tunable wavelength selection.

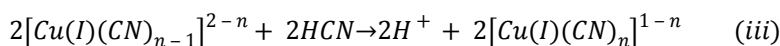
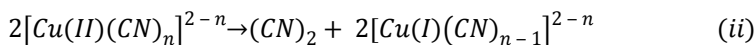
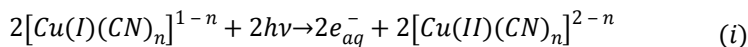
Several of our control experiments were performed with irradiation from a Rayonet photochemical reactor (RPR-200, Figure S2). The lamps used here output the same type of irradiation used by Ritson and Sutherland<sup>1</sup>. This system only allows for irradiation at a wavelength specified by the lamps, which in this case were mercury emission lamps, with primary emission at 254 nm. While the wavelength selection of such systems is rather poor at simulating a prebiotic UV-environment, these systems have the advantage of delivering high fluxes, which can increase reaction rates.



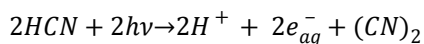
Figure S2. The Rayonet RPR-200 Photochemical Reactor has a maximum of 16 lamps surrounding a central reaction chamber. The lamps used in this study were mercury emission lamps, with primary emission at 254 nm. This reactor is the same system as used by Ritson and Sutherland<sup>1</sup>.

## II. Cyanocuprate Mechanism

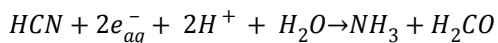
Taking the aqueous solutions to be composed of cyanocuprate species with  $n$  cyanides per copper(I), we can write the steps of the cycle as:



The net reaction is:



The free HCN present in solution at equilibrium acts as a scavenger for the solvated electrons, preventing their recombination with the oxidized copper centers, according to the following equation.



As a consequence of the fact that HCN is limiting and is being depleted from solution as the photoprocess progresses, reaction (iii) becomes inhibited, and the concentration of the cyanocuprate species with higher coordination numbers of cyanide begins to decrease. By monitoring the concentration of cyanocuprate species over time, we can quantify the apparent rate of the cycle.

The absorbance and concentration of cyanocuprate species are related by:

$A = \epsilon lc$ , where  $A$  is the absorbance,  $\epsilon$  is the extinction coefficient,  $l$  is the path length, and  $c$  is the concentration. Differentiating with respect to time gives:

$$\frac{dA}{dt} = \epsilon l \frac{dc}{dt}$$

Thus, the change in concentration with time is related to the change in absorbance with time as:

$$\frac{dc}{dt} = \frac{\frac{dA}{dt}}{\epsilon l}$$

The initial rates of the reactions were all measured in this fashion. We monitored the reaction at 234 nm. We used a standard curve to relate absorbance at 234 nm to concentration of cyanocuprate complexes. The extinction coefficients of the evolving compounds, like cyanogen and formaldehyde, are negligible in this region, in comparison with those of the cyanocuprates. We then assumed that the rate of solvated electron production is proportional to the observed decrease in cyanocuprate complexes.

### **III. UV-Vis Spectroscopy**

#### *a. Irradiation experiments analysis*

For the irradiation wavelength experiments, UV-Vis spectra were obtained with an Amersham Science Ultrospec 3100 Pro over the span of 3.5 hours of irradiation, as described in Section I. The absorption spectrum of the copper cyanide solution contains maxima at 210 and 234 nm. We elected to use the 234 nm feature to look at the kinetics of the reaction. The concentration, as determined by the absorption at 234 nm, was plotted as a function of time. This plot gave a linear trend, which was fit using a python

fitting routine. The slope of this trendline corresponds to the negative rate of the photochemical process. This analysis was performed for each of the irradiation wavelength experiments, which included triplicate studies of each wavelength in the 215–295 nm range in 10 nm intervals. The rates from the triplicate set were averaged to obtain the overall rate, and errors were calculated from the standard deviation of the set. These rates for each irradiation wavelength, however, are not yet comparable, due to varying photon fluxes emitted by the lamp at different wavelengths.

The photon flux at each wavelength was calculated by measuring the power from the lamp at a given wavelength with a ThorLabs power detector. The photon flux is then calculated as the power divided by the energy of a photon at that wavelength ( $E=hc/\lambda$ ). We thus find the photon fluxes for each irradiation wavelength.

In a control experiment, we held the irradiation wavelength constant and varied the photon flux by changing the bandwidth of the tunable lamp setup. This experiment was done with 0.0625 mM copper cyanide, and 0.125 mM potassium cyanide at 235 nm. The rate of the reaction was plotted against the photon flux, and the trend was consistent with an approximate linear dependence (Figure S3). Nonlinear behavior of the rate with photon flux is possible, but this experiment suggested the effect, if any, would be negligible under the range of photon fluxes investigated here. The reaction rates were then normalized by dividing out the incident photon flux, resulting in reaction rates that could be accurately compared.

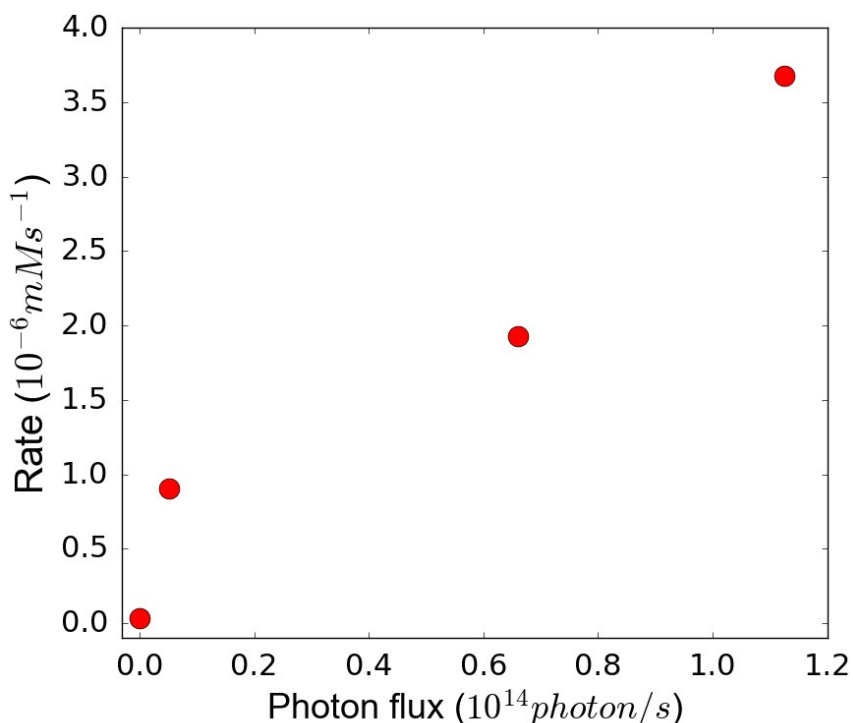


Figure S3. Rate of the cyanocuprate photochemical process, as determined by UV-Vis absorption spectra, for a constant irradiation wavelength of 235 nm, with photon flux varied by changing the bandwidth.

*b. Dicyanocuprate vs. tricyanocuprate*

The number of cyanide ligands coordinated to the copper(I) metal center can vary, generally between zero and four. Past studies of cyanocuprates find that the amount of tetracyanocuprate in solution is exceedingly low<sup>2</sup>, so we neglect this species. Furthermore, the monocyanoocuprate is insoluble and is assumed to precipitate out of solution rapidly when the CN<sup>-</sup> anion is limiting. Thus, we restrict ourselves to di- and tricyanocuprates. Past studies on the photoactivity of each species have produced ambiguous and conflicting results<sup>2,3</sup>. We wanted to understand the composition of our solutions, so we carried out a series of titrations. To do these titrations we first prepared a solution of 63  $\mu$ M CuCN and 63  $\mu$ M KCN, and titrated in increasing amounts of

potassium cyanide using a 110 mM solution of KCN. This solution also contained 63  $\mu\text{M}$  of copper(I) in order to keep the concentration of copper(I) constant throughout the titration. We monitored the UV-Vis absorption spectrum from two to ten equivalents of cyanide to copper(I). The spectra of varying equivalences of cyanide to copper are shown in Figure S4.

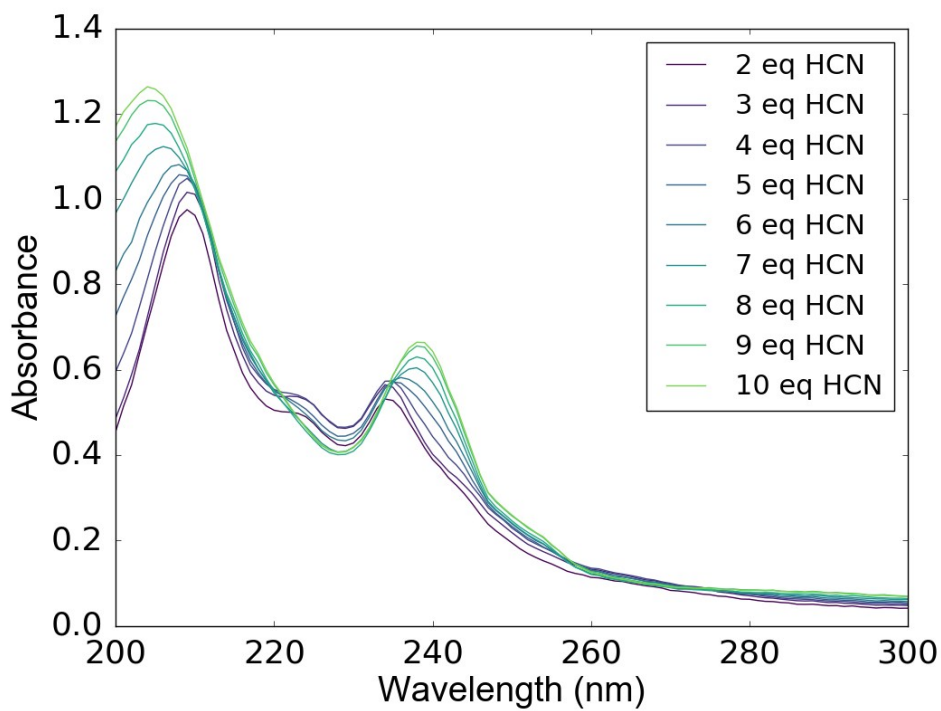


Figure S4. Absorption spectra of cyanocuprate complexes at a range of cyanide to copper(I) ratios. The concentration of copper(I) cyanide was held constant at 0.0625 mM, while the cyanide concentration was varied through titration from 2–10 equivalents of cyanide in total. The pH of the solutions was adjusted to 7.4 and temperature was held constant at 25°C. There are two main morphological spectra found in this range, which are attributed to the dicyanocuprate and tricyanocuprate. The dicyanocuprate spectrum (e.g. 3 equivalents of HCN per copper(I)) has absorption maxima at 210 and 234 nm, with another feature near 220 nm. The tricyanocuprate spectrum (e.g. 8 equivalents of HCN per copper(I)) has absorption maxima at 205 and 239 nm, with the feature at 220 nm gone.

We found two morphologically different spectra, which agree with past literature claims of the spectra of dicyanocuprate and tricyanocuprate<sup>4</sup>. The transition point between these two spectra occurred around six equivalents of potassium cyanide. At lower equivalents of potassium cyanide, the spectrum shows maxima at 210 and 234 nm, with another feature around 220 nm. The tricyanocuprate spectrum has maxima at 205 and 239 nm, with no feature in between. Figure S5 shows the ratio of absorbance at 234 nm to that at 239 nm, as a function of the number of equivalents of potassium cyanide, in order to constrain where the transition point occurs. We find that the ratio of absorbances decreases from roughly 3–6 equivalents of potassium cyanide, before leveling off. This observation indicates that cyanide-to-copper ratios  $>6$  are primarily tricyanocuprate, while those  $<3$  are primarily dicyanocuprate. In the 3–6 range, there is a mixture of the two species.

Our solutions for the irradiation wavelength experiments have a cyanide-to-copper ratio of 3. These solutions should contain a majority of dicyanocuprate species, but with some amount of tricyanocuprate, as indicated by this titration. Further experiments are needed to determine if there are differences in the photoactivities of the two species.

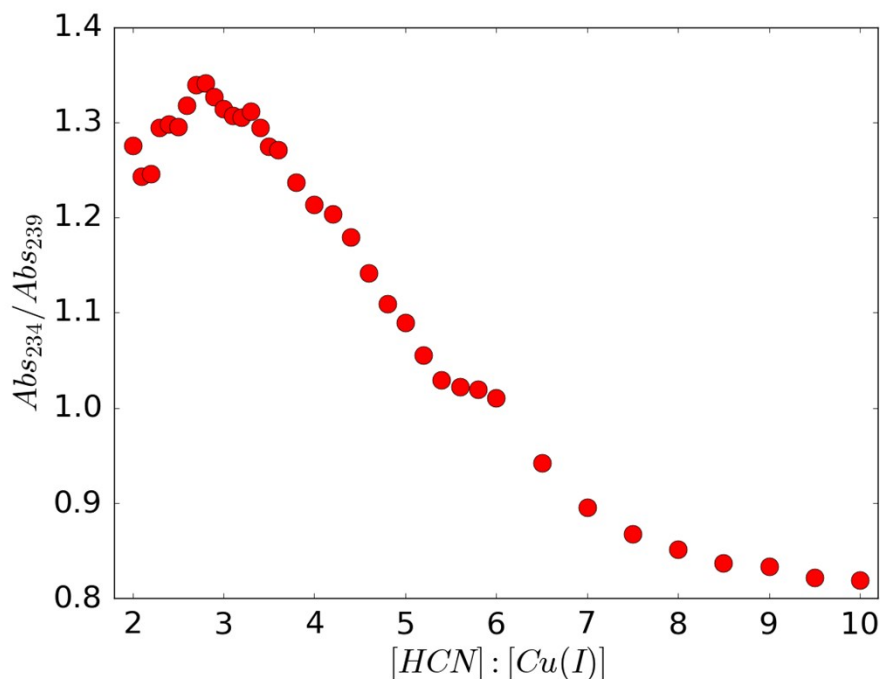


Figure S5. Ratio of absorbances at 234 nm and 239 nm as a function of cyanide-to-copper ratio. The 234 nm feature is attributed to the dicyanocuprate species, while the 239 nm feature is due to the tricyanocuprate. At increasing cyanide-to-copper ratios, the tricyanocuprate feature becomes stronger, as is expected. The transition between species occurs from a cyanide-to-copper ratio of approximately 3–6. The concentration of copper (I) cyanide in these solutions was held at 0.0625 mM, while the total cyanide concentration ranged from 2-10 equivalents of cyanide per copper. The pH was adjusted to 7.4 and temperature was held constant at 25°C.

### *c. Copper control experiments*

In order to make sure that direct photolysis of HCN was not resulting in decreases in the UV-Vis absorption spectrum and being mistaken for the progress of the reaction, we performed a control experiment. In this experiment, a sample of 0.3125 mM HCN (made by adjusting the pH of a 0.3125 mM solution of KCN to pH = 7.4) was prepared and separated into two fractions. One fraction was irradiated in the tunable lamp at 235 nm, while the other was kept in the dark. After 25 hours of irradiation, copper(II) sulfate was added (0.0625 mM) to both the irradiated and dark samples. Copper(II) sulfate was

used because it is a more soluble form of copper when the cyanide anion is limiting. When copper(II) is added to the solution, the copper(II) cyanide complexes that form are unstable and undergo elimination of cyanogen in a bimolecular fashion in order to restore the copper(I) oxidation state. Thus, when copper(II) sources are added, one equivalent of cyanide per copper(II) atom should be consumed in cyanogen production. The remaining cyanide forms copper(I) cyanide complexes, which we measure by UV-Vis absorption spectra. The UV-Vis absorption spectra of these two solutions and found that they were nearly identical (See Figure S6). This observation indicated that there was very little direct photolysis of cyanide during the irradiation. If a significant amount of cyanide had been photolyzed directly, there would not have been enough cyanide ligand in solution to complex the copper species and create similar amounts of absorption as the unirradiated sample. Given that the two spectra are nearly identical, we conclude that hydrogen cyanide photolysis was not of concern on the order of 25 hours of irradiation. Thus, the decreases in the absorption spectrum when solutions of copper cyanide were irradiated are not due to cyanide photolysis and instead are attributed to the progress of the cyanocuprate photochemical process.

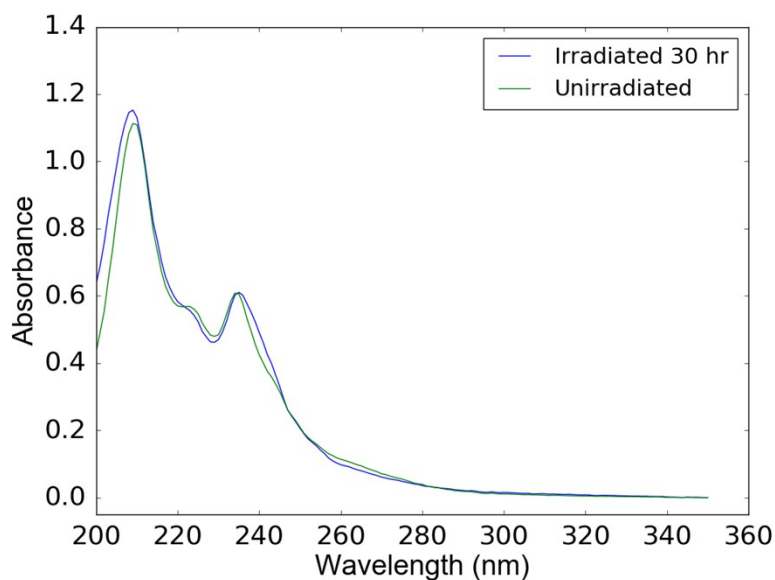


Figure S6. Absorption spectra of the control experiment to test for the photolysis of cyanide. A 0.3125mM KCN solution, pH 7.4, was separated into two fractions; one was irradiated in the tunable lamp at 245 nm for 30 hours while the other was kept in the dark. Then, copper(II) sulfate was added to each sample to give a concentration of 0.0625mM Cu(II). Copper(II) sulfate was used as a more soluble source of copper at low cyanide concentrations. The copper(II) centers eliminate cyanogen in a bimolecular fashion to convert into copper(I) centers. The baselines were adjusted such that the absorbance at 350 nm was set to 0. The absorption spectra of the two samples are very similar, indicating that very little photolysis of cyanide occurs throughout irradiation.

#### IV. Cyanide Electrode Monitoring

In order to further confirm our measurement of the reaction rates with UV-Vis absorption, we additionally monitored the apparent reaction rate as a function of wavelength using both UV-Vis spectroscopy and a cyanide-selective electrode (Fisher Scientific Cyanide Solid-State Combination ISE; BNC connector; catalog number 13-620-538). We repeated experiments in triplicate at the same wavelengths tested previously (215-295 nm, 10 nm intervals, 10 nm bandwidth), monitoring by both UV-Vis absorption and the cyanide probe. For these experiments, solutions of 63  $\mu\text{M}$  CuCN and 125  $\mu\text{M}$  KCN, pH 7.4, were prepared anaerobically and frozen until use. For each

timepoint (0, 30, 60, and 120 minutes), 0.7 mL of solution were thawed and transferred anaerobically to the quartz cuvette for irradiation. An initial UV-Vis absorption spectrum was taken prior to irradiation for the appropriate amount of time. After that time elapsed, a final UV-Vis absorption spectrum was taken and the cuvette was then transferred anaerobically into the oxygen-free glove box. Next, the solution was diluted two-fold to give a total volume of 1.4 mL. We followed the procedure outlined in the cyanide probe manual for dealing with complexes of metal cyanides. Namely, 25  $\mu$ L of acetic acid were added to the 1.4 mL solution to bring it to pH~4. Then, 56  $\mu$ L of 0.5 M EDTA, pH 8 were added to bring the total EDTA concentration to 0.02 M. The solution was vortexed and allowed to sit for 20 minutes to allow for chelation of the copper ions. At this point, the majority of the cyanide was assumed to be free from copper complexes. A standard curve made from cyanide solutions of known concentrations was used to calibrate the total amount of cyanide in the solutions. The samples prior to irradiation generally had cyanide concentrations of 0.11-0.12 mM, as measured by the probe. The total amount of cyanide initially put in the solutions was 0.1875 mM, so roughly 2/3 of the cyanide is detected by the probe. The difference may be due to an equilibrium between chelated and free cyanide or losses brought on by the chelating procedure. Letting the solution sit for longer amounts of time did not significantly change the concentration of cyanide reported by the probe. We also tested for cyanide loss due to volatilization from the acidification step and found this to contribute negligible loss of cyanide. After adding EDTA and allowing time for chelation, 250  $\mu$ L of 10 M KOH were then added to bring the pH of the solution to roughly 10. The cyanide concentration was then determined from the cyanide probe, which had been calibrated with a standard curve of known potassium cyanide

concentrations. The same procedure was repeated for each time point, which began from a fresh sample of the initial solution. Rates were determined from the UV-Vis data as described previously. These rates were in agreement with our past determinations of rates from UV-Vis absorption monitoring at these irradiation wavelengths. Rates were also determined from the cyanide probe readings, which were converted to a free cyanide concentration using a standard curve and corrected for the appropriate dilution factor.

The cyanide probe measures the rate of consumption of cyanide, while the UV-Vis absorption measures the concentration of cyanocuprate species. Depending on the detailed mechanism of the cyanocuprate cycle, a range of number of cyanides per cyanocuprate can be consumed. We estimate that this ranges from 0.5-2 cyanides per cyanocuprate complex, based on the suggested mechanism in Ritson & Sutherland<sup>1</sup>. This factor will influence the difference between the rates measuring the cyanocuprate vs. free cyanide concentrations. Since the detailed mechanism of the cycle is not definitively known, we do not adopt a correction factor for this fact and instead directly compare the measured rates, with the assumption that these rates should not agree precisely.

These experiments were performed in triplicate at all wavelengths. The probe consistently measured higher rates than the absorbance method, which is consistent with our expectations due to the consumption of multiple cyanide molecules per cyanocuprate as the cycle turns. Figure S7 shows the relative rate at each wavelength as determined by both the absorbance and probe methods. While the numerical values are not precisely correlated, the overall trend is consistent; namely, the cyanocuprate protoprocess is more efficient at shorter wavelengths. Wavelengths below 250 nm are 2.8 and 4.0 times faster than those above 250 nm for the probe and absorbance methods, respectively.

Furthermore, the rates we monitored with the two different methods show the same overall wavelength trend and are in general agreement when considering the unknown correction factor from the details of the mechanism and the errors inherent in the experiments.

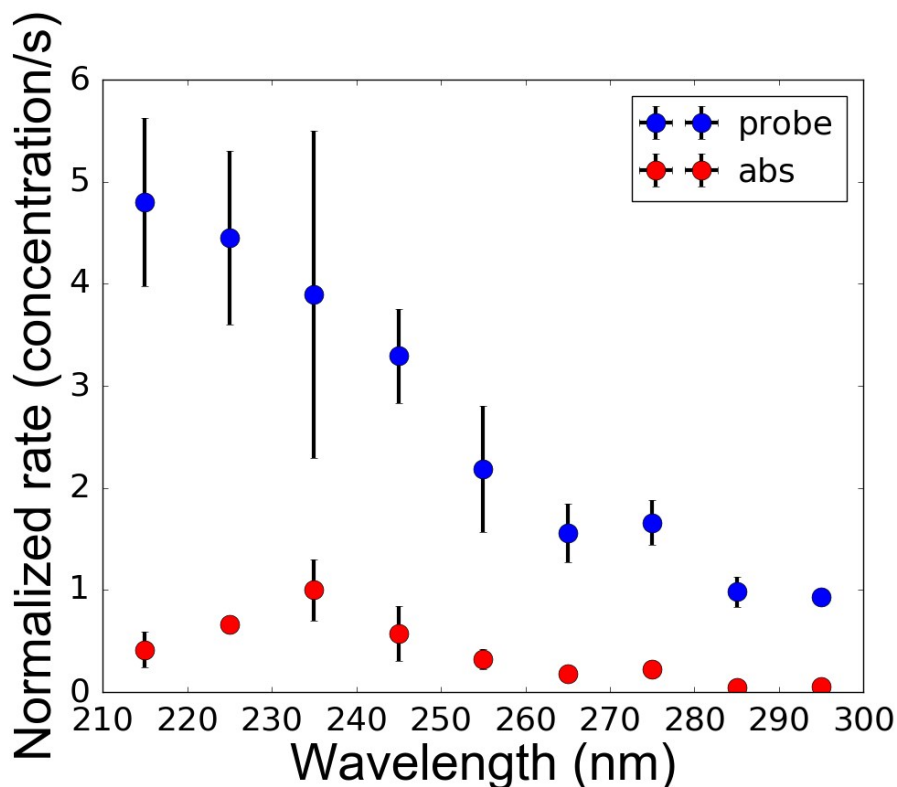
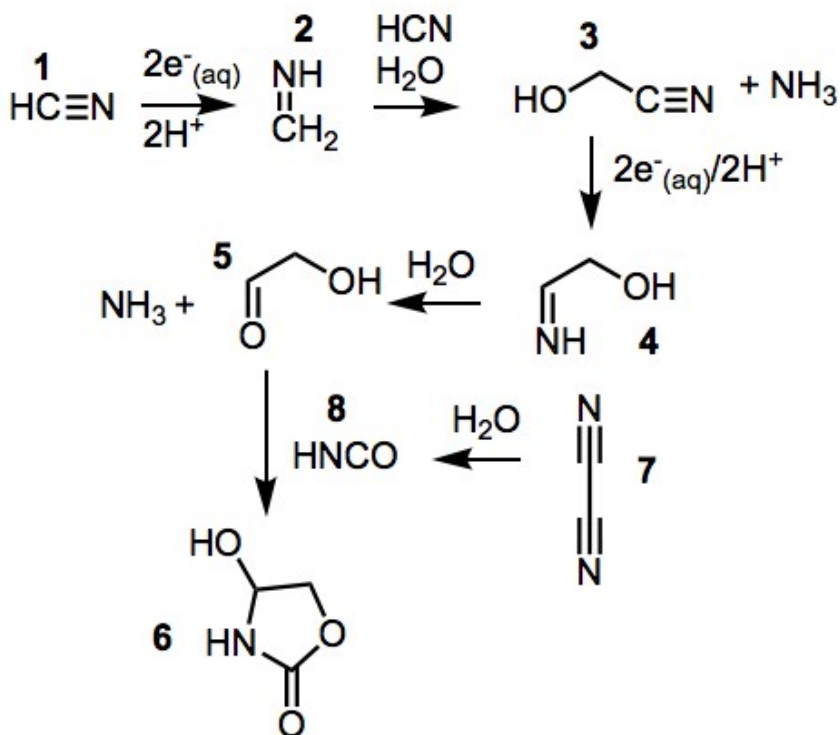


Figure S7. Relative rate of the reaction as a function of incident wavelength, normalized by photon flux, as determined by both the cyanide electrode (blue) and absorbance measurements (red). Each experiment was completed in triplicate (as described above). The points represent the average of the triplicate set, and the error bars are the error from the triplicate set. The cyanide electrode consistently measures a higher rate, due to detecting the total cyanide concentrations, while the absorbance method measures the concentration of cyanocuprate complexes. The overall wavelength dependence from the two methods is broadly consistent: the relative rate of the reaction is generally larger at lower wavelengths. The numerical values (and errors) for data presented here are located in section VII.

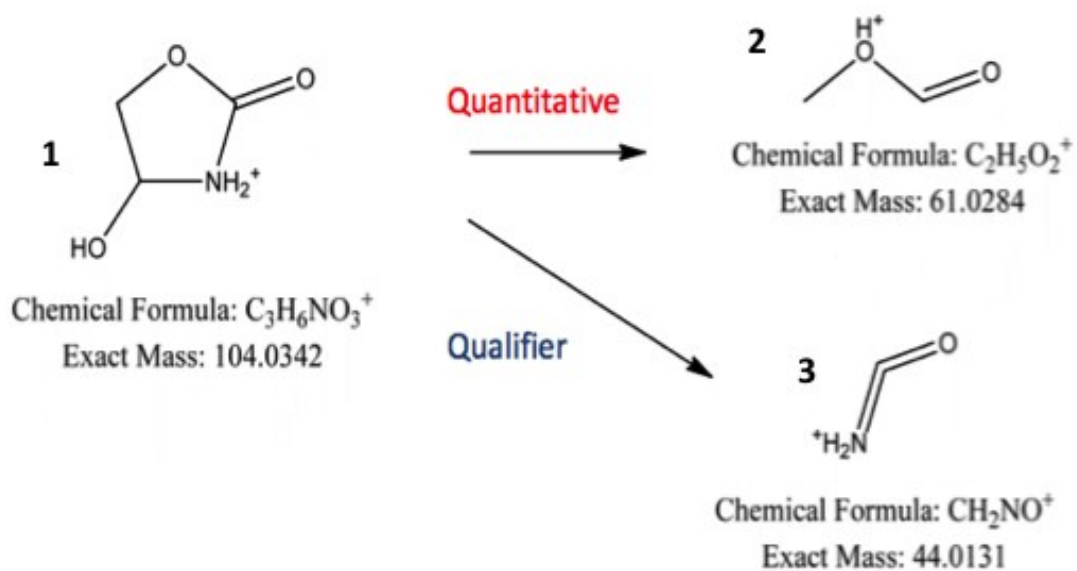
## V. LC-MS

While we used UV-Vis absorption spectroscopy to analyze the kinetics of the reaction, we also monitored the products of the reaction by LC-MS (Agilent 6460 Triple Quad LC/MS with Agilent 1290 Infinity HPLC). Ritson and Sutherland<sup>1</sup> identify the major products of the reaction after prolonged irradiation as the glycolaldehyde and glyceraldehyde derived 4-hydroxyoxazolidin-2-one and 4-hydroxy-5-(hydroxymethyl)oxazolidin-2-one, respectively (Scheme S1). The 4-hydroxyoxazolidin-2-one (**6**) should always be produced in higher yields, so we elected to detect that compound. We synthesized a standard of **6** using the procedure of Ritson and Sutherland<sup>1</sup>. We calibrated the concentration of this standard using <sup>1</sup>H-NMR with an NMR tube containing a coaxial insert filled with triethylamine as a standard for integration. An LC-MS method was developed to detect the product using a 4.6 x 50 mm Gemini C18 5 μm column. The flow rate was 0.3 mL/min and an injection volume of 5 μL was used and eluting solvents were A) water with 0.1% formic acid, and B) acetonitrile with 0.1% formic acid. We submitted samples (0.25 mM CuCN, 0.75 mM KCN, pH 7.4) for LC-MS analysis after prolonged irradiation (~70–76 hours) at each irradiation wavelength. The [M+H]<sup>+</sup> parent compound, C<sub>3</sub>H<sub>6</sub>NO<sub>3</sub><sup>+</sup> (mass of 104) produced two fragments: CH<sub>2</sub>NO<sup>+</sup> (the “qualifier” compound, mass of 44) and C<sub>2</sub>H<sub>5</sub>O<sub>2</sub><sup>+</sup> (mass of 61), which was used for quantitative analysis (Scheme S2). The quantifier was chosen due to its higher abundance. The qualifier is used as a measure of enhanced selectivity and to reduce the chance of false positives. The synthesized standard was analyzed under the above conditions, and found to have a retention time of roughly 2.93 minutes (Figure S8). Irradiated samples produced peaks at the same retention time,

followed by a closely eluting background peak. The peak from the target compound was integrated to avoid interference from the background peak, as shown in Figure S9. The results showed the detection of the target compound above the threshold detection limit for all irradiation wavelengths, except for the negative control of 320 nm. See Table S1 for yields at various irradiation wavelengths. This set of experiments confirmed that the reaction proceeds in the same manner towards producing the same products at all irradiation wavelengths between 200 and 300 nm.



Scheme S1: The systems chemistry process that occurs during this reaction reduces hydrogen cyanide **1** first to methanimine **2** by action of solvated electrons. Methanimine hydrolyzes to formaldehyde which reacts with HCN to yield cyanohydrin **3**, and this product undergoes further reduction by solvated electrons to imine **4**. Glycolaldehyde **5** is produced by another round of homologation. Oxazolidinone **6** forms by cycloaddition of glycolaldehyde with cyanic acid **8**, a product produced by hydrolysis of cyanogen **7**. **6** accumulates in solution and is the product we detect by LC-MS.



Scheme S2: Fragmentation of the protonated oxazolidinone (mass of 104) to the fragment used for quantification ( $C_2H_5O_2^+$ , mass of 61) and the qualifier fragment ( $CH_2NO^+$ , mass of 44). The target compound, **1**, was fragmented into **2** and **3**. Quantification was performed using compound **2**.

Table S1: LC-MS detection of oxazolidinone at various irradiation wavelengths

Wavelength (nm)	Yield ( $\mu$ M)	Irradiation time (hours)	Wavelength (nm)	Yield ( $\mu$ M)	Irradiation time (hours)
210	0.56	75	255	0.56	74
220	0.09	73	265	1.01	72
230	0.42	70	275	0.19	72
240	1.17	72	285	0.21	77
247	0.26	73	295	0.02	74.5

0.1  $\mu\text{M}$  standard

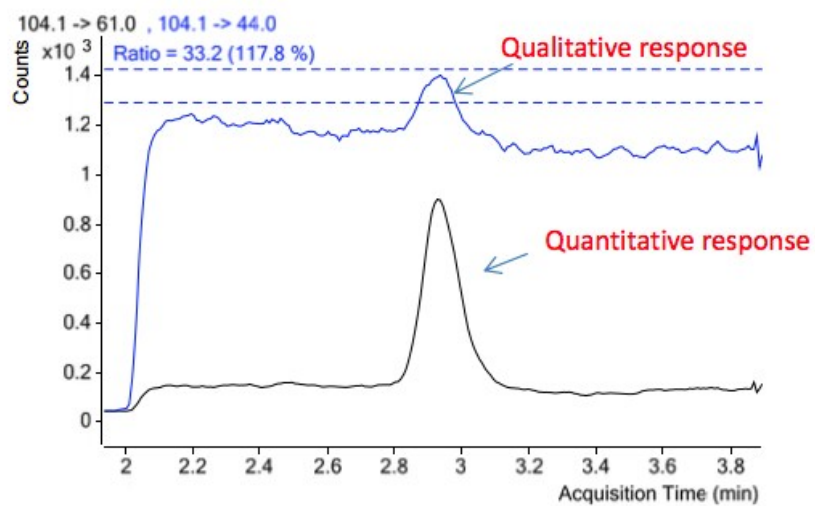


Figure S8: LC-MS chromatogram for a synthetically prepared standard of 0.1  $\mu\text{M}$  of **6**. The black curve shows the trace for the quantifying fragment (mass of 61), while the blue shows that of the qualifier fragment (mass of 44).

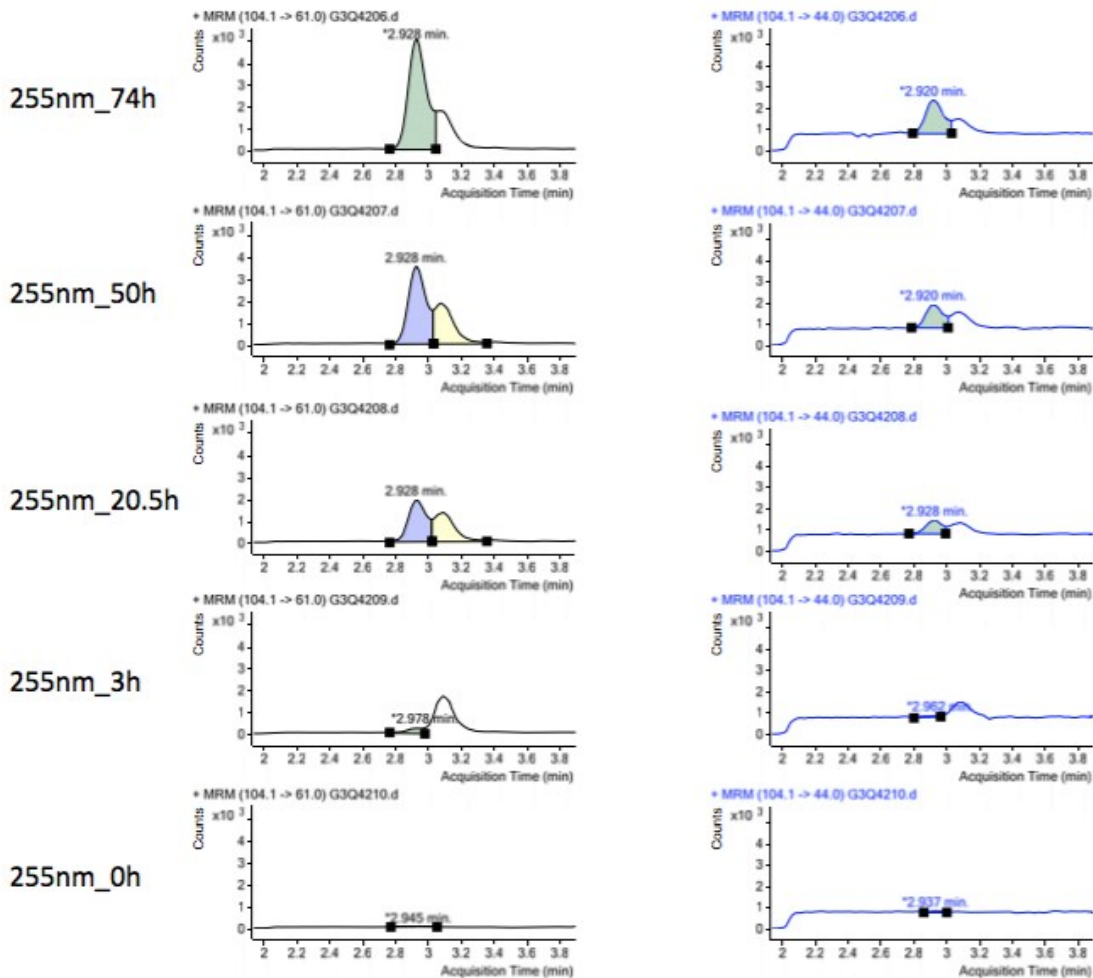


Figure S9: Sample LC-MS chromatograms for 255 nm irradiation. The experiment was sampled at times of 0, 3, 20.5, 50, and 74 hours. The black curves show the quantifying fragment (mass of 61), while the blue curves show the qualifier fragment (mass of 44). The appropriate peak was identified and calibrated by standards of synthesized oxazolidinone **6** ( $C_3H_6NO_3^+$ ). The peak eluting behind the peak of the target is likely due to a background molecule and does not affect the results.

## VI. Atmospheric Modeling

When carrying out the calculation of weighted surface intensity, we used code produced and described in Ranjan and Sasselov<sup>5</sup>. This code takes as input a user-specified atmospheric profile (composition, temperature, and pressure), and runs it through a two-stream clear-sky radiative transfer model to compute relevant spectral quantities, including total surface flux and total surface intensity. The total surface

radiance from the model was integrated in 10 nm wavelength bins to get the total surface radiance value to multiply by the normalized relative reaction rates (or action spectrum), in order to get the relative rate of solvated-electron production. These values were normalized such that the maximum was equal to 1. The normalized rates plotted against irradiation wavelength are often referred to as an action spectrum, which is a measure of the activity of a reaction as a function of wavelength. The two atmospheres selected for use in this study include the modern Earth atmosphere and a sample prebiotic atmosphere, from Rugheimer et al.<sup>6</sup> The exact chemical compositions of these atmospheres can be found in Figure 3a of the main text.

## VII. Tables of Experimental Values

The numerical values (with associated errors) for data found in Figures 1c, 2, and S7 are presented in the tables below.

Table S2: Data for Figure 1C: normalized rate vs. wavelength.

Wavelength (cm)	Rate ([CuCN <sub>n</sub> ]/s)	Error ([CuCN <sub>n</sub> ]/s)
215	0.991	0.16
225	1	0.21
235	0.918	0.19
245	0.837	0.16
255	0.204	0.021
265	0.0696	0.032
275	0.0744	0.023
285	0.0321	0.0064
295	0.0278	0.004

Table S3: Data for Figure 2: Normalized quantum yield vs. wavelength

Wavelength (nm)	Quantum Yield	Error
215	0.878	0.15
225	0.958	0.2
235	0.853	0.18
245	1	0.2
255	0.332	0.036
265	0.134	0.065
275	0.171	0.054
285	0.089	0.018
295	0.086	0.013

Table S4: Data for Figure S7: Normalized rate vs. wavelength for probe and absorbance experiments.

Wavelength (nm)	Probe		Absorbance	
	Average (conc/s)	Error (conc/s)	Average (conc/s)	Error (conc/s)
215	4.8	0.83	0.415	0.17
225	4.45	0.85	0.661	0.073
235	3.89	1.6	1	0.3
245	3.29	0.46	0.57	0.27
255	2.18	0.62	0.322	0.099
265	1.56	0.29	0.179	0.043
275	1.66	0.22	0.219	0.046
285	0.98	0.15	0.0477	0.016
295	0.935	0.056	0.0533	0.025

### VIII. References

- 1 D. Ritson, J.D. Sutherland, *Nat. Chem.*, 2012, **4**, 895.
- 2 A. Horvath, S. Papp, Z. Decsy, *J. Photochem.*, 1984, **24**, 331.
- 3 A. Horvath, Z. Zsilak, S. Papp, *J. Photochem. Photobiol.*, 1989, **50**, 129.
- 4 J. H. Baxendale and D.T. Westcott, *J. Am. Chem. Soc.* 1959, 2347.
- 5 S. Ranjan, D.D. Sasselov, *Astrobiology*, 2017, **17**, 169.
- 6 S. Rugheimer, A. Segura, L. Kaltenegger, D. Sasselov, *Astrophys. J.* **2015**, 806, 137.